AIAA SciTech Forum
8–12 January 2018, Kissimmee, Florida
2018 AIAA Aerospace Sciences Meeting

10.2514/6.2018-0592

Wavelet-based delayed detached eddy simulation method for compressible wall bounded turbulent flow modeling

Xuan Ge*[1], Oleg V. Vasilyev†[2,3,4], and M. Yousuff Hussaini‡[1]

[1] *Florida State University, Tallahassee, FL 32306, USA*
[2] *Skolkovo Institute of Science and Technology, Moscow 143026, Russia*
[3] *NorthWest Research Associates, Boulder CO 80301, USA*
[4] *University of Colorado, Boulder CO 80309, USA*

A novel Wavelet-based adaptive Delayed Detached Eddy Simulation (W-DDES) approach for simulations of wall-bounded compressible turbulent flows is proposed. The new approach utilizes anisotropic wavelet-based mesh refinement and its effectiveness is demonstrated for flow simulations using the Spalart-Allmaras DDES model. A variable wavelet thresholding strategy blending two distinct thresholds for the Reynolds-averaged Navier-Stokes (RANS) and Large-Eddy Simulation (LES) regimes is used. A novel mesh adaptation on mean and fluctuation quantities with different wavelet threshold levels is proposed. The new strategy is more accurate and efficient compared to the adaptation on instantaneous quantities using *a priori* defined uniform thresholds. The effectiveness of the W-DDES method is demonstrated by comparing the results of the W-DDES simulations with results already available in the literature. A supersonic plane channel flow is tested as a benchmark wall-bounded flow. Both the accuracy indicated by the threshold and efficiency in terms of degrees of freedom for the novel adaptation strategy are successfully gained compared with the wavelet-based adaptive LES method. Moreover, the newly proposed W-DDES resolves the typical log-layer match issue encountered in the conventional non-adaptive DDES method mainly due to the use of wavelet-based adaptive mesh refinement. The current study serves as a crucial step towards construction of a unified wavelet-based adaptive hierarchical RANS/LES modeling framework, capable of performing simulations of varying fidelities from no-modeling direct numerical simulations to full-modeling RANS simulations.

I. Introduction

The latest advancements in wavelet-based numerical methodologies to solve partial differential equations,[1–5] combined with the unique properties of wavelet analysis to identify and isolate localized dynamically dominant flow structures,[6,7] and to track them on adaptive computational meshes,[8–12] have demonstrated the benefits of using spatio-temporal mesh adaptation for numerical simulations of turbulent flows. The wavelet-based methods with inherent adaptive mesh refinement capabilities and sparse data representation not only take full advantage of spatio-temporal intermittency of turbulent flows by substantially reducing the number of degrees of freedom and, consequently, the computational cost, but also provide a systematic framework for active error control.

Further tight integration of an adaptive wavelet-based method with turbulence modeling allows a construction of a hierarchical framework for simulating turbulent flows[13] where coherent flow structures are either totally or partially resolved on self-adaptive computational grids, while modeling the effect of unresolved motions. The separation between resolved (more energetic) eddies and residual (less energetic) flow

*Postdoctoral Scholar, Department of Mathematics, Florida State University
†Professor, Center for Design, Manufacturing and Materials, Skolkovo Institute of Science and Technology; Sr. Research Scientist, NorthWest Research Associates;
Professor, Department of Mechanical Engineering, University of Colorado, AIAA Senior Member
‡Professor of Mathematics and Computational Science & Engineering, AIAA Fellow

is achieved by means of the nonlinear wavelet thresholding filter. The value of wavelet threshold controls the relative importance of resolved field and residual background flow and, thus, the fidelity of turbulence simulations. By increasing the thresholding level a unified **hierarchy** of wavelet-based turbulence models of different fidelity can be obtained. Wavelet-based direct numerical simulation (WDNS), coherent vortex simulation (CVS)[6] and wavelet-based stochastic coherent adaptive large-eddy simulation (SCALES),[7] also referred to as Adaptive LES, represent different fidelity methods within this hierarchy. A distinct advantage of the adaptive wavelet-based hierarchical framework is that the overall physical fidelity of the simulation can be simply controlled by the adaptive wavelet threshold filter,[14,15] thereby providing a fully unified hierarchical modeling framework that allows transition continuously among various fidelities, from WDNS to CVS to Adaptive LES, and even to Wavelet-based Adaptive Unsteady RANS (W-URANS) simulations.[16]

Transition from DNS to CVS to Adaptive LES is well established through controlling the wavelet threshold. WDNS uses wavelet-based discretization of the Navier-Stokes equations to adapt dynamically the local resolution of intermittent flow structures.[12,17,18] Transition from WDNS to CVS[6] is achieved by using an optimal wavelet threshold, resulting in the decomposition of the flow field into coherent and incoherent contributions. For Adaptive LES, the wavelet threshold is further increased so that the stochastic and the least energetic coherent portion of the turbulent solution are discarded and only the most energetic part of the coherent vortices are captured in the resolved field.[7] In adaptive LES methods, similar to conventional LES, the discarded subgrid-scale (SGS) coherent structures dominate the total SGS dissipation.[7,19] Therefore, many standard LES closures are applicable for the Adaptive LES method.

The transition to the W-URANS regime is not as straightforward. In RANS equations, the unknown variables are mean (Reynolds-averaged or Favre-averaged) quantities, which are smooth and whose evolution is described by dissipative models. As shown in Ref. 16, the accurate solution of RANS equations, even on adaptive meshes as in W-URANS, requires the use of low wavelet threshold values compared to the ones used in WDNS, which is counterintuitive when compared to the monotonically increasing threshold value for decreasing fidelity from the WDNS to CVS to Adaptive LES regimes. The objective of the present study is to develop a hybrid mathematically consistent approach with coexistence, connection and even active communication between the W-URANS and Adaptive LES regions. The current work serves as a crucial step towards construction of a unified wavelet-based adaptive hierarchical RANS/LES modeling framework, capable of performing simulations of various fidelity from no-modeling direct numerical simulations to full-modeling RANS simulations.

It is important to emphasize that in contrast to conventional hybrid RANS/LES methods where the grid is specified *a priori*, our approach uses a dynamically adaptive grid. A variable wavelet thresholding strategy blending two distinct thresholds for the W-URANS and Adaptive LES regimes is used. In addition, a novel mesh adaptation on mean and fluctuation quantities with different wavelet thresholds levels is proposed. The effectiveness of the W-DDES method is demonstrated by comparing the results of the W-DDES simulations with the results already available in the literature. A supersonic plane channel flow are tested as a benchmark wall-bounded flow.

This paper is organized as follows. Section II introduces the governing equations of the simulations, including the Favre-filtered Navier-Stokes equations for compressible flows and the evolution equations for turbulence models. The wavelet-based adaptive methods and the Adaptive-Anisotropic Wavelet Collocation Method (A-AWCM) for complex domain geometries are described in Section III. Section IV describes the novel adaptation strategy treating different flow regimes and mean and fluctuation quantities elaborately. The simulations setup and corresponding results are presented and discussed in Section V. Concluding remarks are given at the end in Section VI.

II. Governing Equations

II.A. Favre-filtered Navier-Stokes equations

For compressible flows, the W-URANS formulations are in terms of Reynolds-averaged and Favre-averaged dependent variables, whereas the adaptive LES formulations are in terms of wavelet-based grid-filtered and Favre-filtered dependent variables. For the sake of simplicity, we use the term "Favre-filtered" for all dependent variables in the W-DDES formulations. The Favre-filtered Navier-Stokes equations for conservation of

mass, momentum, and energy in compressible flows with modeled turbulent terms are written below.

$$\frac{\partial \rho}{\partial t} + \frac{\partial (\rho u_j)}{\partial x_j} = 0, \tag{1}$$

$$\frac{\partial \rho u_i}{\partial t} + \frac{\partial}{\partial x_j}\left(\rho u_i u_j\right) = -\frac{\partial p}{\partial x_i} + \frac{\partial \hat{\tau}_{ij}}{\partial x_j}, \tag{2}$$

$$\frac{\partial \rho e}{\partial t} + \frac{\partial}{\partial x_j}\left[\left(\rho e + p\right) u_j\right] = \frac{\partial}{\partial x_j}\left[u_i \hat{\tau}_{ij} - q_j\right], \tag{3}$$

where

$$p = \rho R T, \tag{4}$$

$$e = \frac{1}{2} u_i u_i + \frac{p}{\rho(\gamma - 1)}, \tag{5}$$

$$q_j = -c_p \left(\frac{\mu}{Pr_L} + \frac{\mu_T}{Pr_T}\right) \frac{\partial T}{\partial x_j}, \tag{6}$$

$$\begin{aligned} \hat{\tau}_{ij} &= 2\mu \tilde{S}_{ij} + \tau_{ij}, \\ \tau_{ij} &= 2\mu_T \tilde{S}_{ij}, \\ \tilde{S}_{ij} &= dev(S_{ij}) = S_{ij} - \frac{1}{3}\frac{\partial u_k}{\partial x_k}\delta_{ij}, \\ S_{ij} &= \frac{1}{2}\left(\frac{\partial u_i}{\partial x_j} + \frac{\partial u_j}{\partial x_i}\right), \end{aligned} \tag{7}$$

where ρ is the the wavelet-based grid-filtered density of the fluid (gas), p is the wavelet-based grid-filtered pressure, ρu_j is the mass flux, u_j is the Favre-filtered velocity, T is the Favre-filtered temperature, and e is the Favre-filtered total energy per unit mass. Parameter R is the gas constant, while c_v and c_p are the specific heats at constant volume and pressure, respectively. The specific heat ratio $\gamma = \frac{c_p}{c_v} \equiv 1.4$ for diatomic gases, and $Pr = \frac{\mu c_p}{\lambda}$ is the Prandtl number. The term q_j is the sum of both the laminar and modeled turbulent heat fluxes with $Pr_L = 0.72$ and $Pr_T = 0.9$ being the laminar and turbulent Prandtl numbers respectively. The turbulent eddy viscosity is denoted by μ_T, which is unknown and needs turbulence models for closure. The term $\hat{\tau}_{ij}$ is the sum of the molecular and Reynolds stress tensors, while τ_{ij} is the Reynolds stress tensor, S_{ij} is the mean strain-rate tensor, and $\tilde{S}_{ij}$ is the deviatoric tensor of S_{ij}. The temperature dependent dynamic molecular viscosity μ is given by the Sutherland's law,

$$\frac{\mu}{\mu_{ref}} = \frac{T_{ref} + S}{T + S}\left(\frac{T}{T_{ref}}\right)^{3/2}, \tag{8}$$

where the constants $S = 110.4K$ and $T_{ref} = 293.15K$.

II.B. Turbulence model equations

The Delayed Detached Eddy Simulation (DDES) model employed in this work is the Spalart-Allmaras (S-A) model based DDES.[20] This model is an improved version of the original DES model[21] with a crucial re-defining of the DES length scale $\tilde{d}$ in terms of a shielding function f_d, which is written as

$$f_d \equiv 1 - \tanh([8 r_d]^3), \tag{9}$$

with its argument r_d given by

$$r_d \equiv \frac{\nu_T + \nu}{\sqrt{u_{i,j} u_{i,j}}\kappa^2 d^2}, \tag{10}$$

where ν_T is the kinematic eddy viscosity, ν the molecular viscosity, $u_{i,j}$ the velocity gradients, κ the Kármán constant, and d the distance to the wall. The parameter r_d is unity in the log-layer, and gradually falls to 0 at the edge of the boundary layer. Therefore, f_d vanishes within the log-layer and increases to 1 out of the boundary layer. Then the length scale $\tilde{d}$ replaces the wall distance d, namely the RANS length scale in the S-A model. $\tilde{d}$ has the form

$$\tilde{d} \equiv l_{RANS} - f_d \max(0, l_{RANS} - l_{LES}) \tag{11}$$

where $l_{RANS} = d$, $l_{LES} = \Psi C_{DES}\Delta$, and Δ is the sub-grid length scale given by maximum local grid spacing among three Cartesian directions in the physical domain, namely

$$\Delta = \max(\Delta_x, \Delta_y, \Delta_z), \tag{12}$$

$C_{DES} = 0.65$ is an empirical constant,[22] Ψ is a low Reynolds number correction[20] given by

$$\Psi^2 = \min\left[10^2, \frac{1 - \frac{c_{b1}}{c_{w1}\kappa^2 f_w^*}[f_{t2} + (1 - f_{t2})f_{v2}]}{f_{v1}\max(10^{-10}, 1 - f_{t2})}\right], \tag{13}$$

$f_w^* = 0.424$ and other constant coefficients follow the original S-A model and are described below. Note that in RANS mode $f_d = 0$, $\tilde{d} = d$, whereas in LES mode $f_d = 1$ and, thus, $\tilde{d} = \min(d, \Psi C_{DES}\Delta)$. Using the blending or shielding function f_d, the RANS mode is shielded or delayed up to the log-layer, whereas for the original DES model, the LES mode may take over the RANS mode earlier below the log-layer at intermediate cell aspect ratios, which causes the modeled-stress depletion (MSD).[20]

The standard Spalart-Allmaras model[23] in terms of $\rho\tilde{\nu}$ is written as

$$\begin{aligned}\frac{\partial \rho\tilde{\nu}}{\partial t} + \frac{\partial}{\partial x_j}(\rho\tilde{\nu}u_j) &= c_{b1}(1 - f_{t2})\tilde{S}\rho\tilde{\nu} - \left[c_{w1}f_w - \frac{c_{b1}}{\kappa^2}f_{t2}\right]\rho\left(\frac{\tilde{\nu}}{\tilde{d}}\right)^2 \\ &+ \frac{\partial}{\partial x_j}\left[\left(\frac{\mu}{\sigma} + \frac{\rho\tilde{\nu}}{\sigma}\right)\frac{\partial\tilde{\nu}}{\partial x_j}\right] - \left(\frac{\mu}{\sigma\rho} + \frac{\tilde{\nu}}{\sigma}\right)\frac{\partial\rho}{\partial x_j}\frac{\partial\tilde{\nu}}{\partial x_j} + c_{b2}\frac{\rho}{\sigma}\frac{\partial\tilde{\nu}}{\partial x_j}\frac{\partial\tilde{\nu}}{\partial x_j},\end{aligned} \tag{14}$$

and the eddy viscosity is computed from:

$$\mu_T = \rho\tilde{\nu}f_{v1} \tag{15}$$

where

$$\begin{aligned} f_{v1} &= \frac{\chi^3}{\chi^3 + c_{v1}^3}, \\ \chi &= \tilde{\nu}/\nu, \\ \tilde{S} &= \max\left[0.3\sqrt{2\Omega_{ij}\Omega_{ij}}, \sqrt{2\Omega_{ij}\Omega_{ij}} + \frac{\tilde{\nu}}{\kappa^2\tilde{d}^2}f_{v2}\right], \\ \Omega_{ij} &= \frac{1}{2}\left(\frac{\partial u_i}{\partial x_j} - \frac{\partial u_j}{\partial x_i}\right), \\ f_{v2} &= 1 - \frac{\chi}{1 + \chi f_{v1}}, \\ f_w &= g\left[\frac{1 + c_{w3}^6}{g^6 + c_{w3}^6}\right]^{1/6}, \\ g &= r + c_{w2}(r^6 - r), \\ r &= \min\left[\frac{\tilde{\nu}}{\tilde{S}\kappa^2\tilde{d}^2}, 10\right], \\ f_{t2} &= c_{t3}\exp(-c_{t4}\chi^2), \end{aligned}$$

and $\tilde{d}$ is the hybrid DDES length scale defined in Eq. (11). To avoid possible numerical problems, Spalart (private communication) suggests limiting $\tilde{S}$ to be no smaller than $0.3\sqrt{2\Omega_{ij}\Omega_{ij}}$. $c_{b1} = 0.1355$, $c_{b2} = 0.622$, $\sigma = 2/3$, $\kappa = 0.41$, $c_{w2} = 0.3$, $c_{w3} = 2$, $c_{v1} = 7.1$, $c_{w1} = \frac{c_{b1}}{\kappa} + \frac{1+c_{b2}}{\sigma}$. This "standard" version of the S-A model does not have the trip term "f_{t1}", and hence it is argued that f_{t2} is not necessary, i.e. $c_{t3} = 0$. The no-slip wall boundary condition for $\tilde{\nu}$ is $\tilde{\nu} = 0$.

III. Wavelet-based Adaptive Computations

The turbulence models described above are implemented using the parallel Adaptive Wavelet Collocation method (AWCM).[5] The unsteady RANS governing equations are evaluated at collocation points, which are adapted in space and time to dynamically resolve all the features of the numerical solution. The essential features of the AWCM are briefly described in the next two sections. For detailed discussion the reader is referred to Refs. 1, 2, 5, 24. A novel treatment of periodic boundary conditions is described in Section III.C.

III.A. Adaptive Wavelet Collocation Method

The Adaptive Wavelet Collocation Method is based on multi-resolution wavelet analysis to construct time-dependent computational meshes with spatially varying resolution, required to adequately capture the localized features of the solution with *a priori* prescribed accuracy. The grid adaptation is based on the analysis of the wavelet decomposition of a spatially dependent field, say $u(\mathbf{x})$, sampled on a set of dyadic nested collocation points $\mathbf{x}^j_\mathbf{k}$ at different levels of resolution j, formally written as

$$u(\mathbf{x}) = \sum_{\mathbf{l}\in\mathcal{L}^1} c^1_\mathbf{l}\phi^1_\mathbf{l}(\mathbf{x}) + \sum_{j=1}^{J-1}\sum_{\mu=1}^{2n-1}\sum_{\mathbf{k}\in\mathcal{K}^{\mu,j}} d^{\mu,j}_\mathbf{k}\psi^{\mu,j}_\mathbf{k}(\mathbf{x}), \tag{16}$$

where n denotes the number of spatial dimensions, bold subscripts denote n-dimensional indices, while $\mathcal{L}^1$ and $\mathcal{K}^{\mu,j}$ are n-dimensional index sets associated with scaling functions $\phi^1_\mathbf{l}$ and wavelets $\psi^{\mu,j}_\mathbf{k}$, respectively. Each of the basis functions, *i.e.* $\phi^1_\mathbf{l}$ or $\psi^{\mu,j}_\mathbf{k}$, corresponds one-to-one with a grid point $\mathbf{l}\in\mathcal{L}^1$ or $\mathbf{k}\in\mathcal{K}^{\mu,j}$. Scaling functions $\phi^1_\mathbf{l}$ carry the averaged signal, while the multi-dimensional second-generation wavelet functions $\psi^{\mu,j}_\mathbf{k}$ define local, variational details. The amplitudes are given by the coefficients $c^1_\mathbf{l}$ and $d^{\mu,j}_\mathbf{k}$, respectively, and hence have a unique correspondence to grid points. Levels of resolution span over $1\leqslant j\leqslant J$, with J being the maximum level present in the approximation (associated to the finest grid resolution). During wavelet transform, detail (or wavelet) coefficients $d^{\mu,j}_\mathbf{k}$ are obtained recursively from scaling coefficients $c^{\mu,j}_\mathbf{k}$ from level $J-1$ to 1. After wavelet transform, grid points $\mathbf{l}\in\mathcal{L}^1$ at the coarsest level store the scaling coefficients $c^1_\mathbf{l}$, and all the other grid points $\mathbf{k}\in\mathcal{K}^{\mu,j}$ at higher levels store the wavelet coefficients $d^{\mu,j}_\mathbf{k}$. To avoid ambiguity, grid points $\mathbf{k}\in\mathcal{K}^{\mu,j}$ with $1\leqslant j\leqslant J-1$ represent all collocation points located at level $2\leqslant j\leqslant J$. Note that for n-dimensional space, there are $2n-1$ families of wavelet functions, μ.

Wavelet threshold filtering arises naturally from the series expansion (16). The filtering operation is performed by applying the wavelet transform to the original field $u(\mathbf{x})$, zeroing the wavelet coefficients below a given threshold, $\epsilon=\epsilon(\mathbf{x},t)$ for generality, and transforming back to the physical space. The resulting approximate field, say $u^{>\epsilon}(\mathbf{x})$, composed of a subset of the original wavelets, represents the dominant modes and formally can be written as the conditional series

$$u^{>\epsilon}(\mathbf{x}) = \sum_{\mathbf{l}\in\mathcal{L}^1} c^1_\mathbf{l}\phi^1_\mathbf{l}(\mathbf{x}) + \sum_{j=1}^{J-1}\sum_{\mu=1}^{2n-1}\sum_{\substack{\mathbf{k}\in\mathcal{K}^{\mu,j}\\ |d^{\mu,j}_\mathbf{k}|>\epsilon\|u(\mathbf{x})\|}} d^{\mu,j}_\mathbf{k}\psi^{\mu,j}_\mathbf{k}(\mathbf{x}). \tag{17}$$

In many implementations, the filter threshold is taken to be relative to some characteristic scale, often represented by either the L_2- or $L_\infty-$ norm of $u(\mathbf{x})$ and denoted as $\|u(\mathbf{x})\|$.[7] The resulting nonlinear filtering operation separates resolved flow structures and unresolved residual motions. For a properly normalized threshold, the reconstruction error of the filtered variable is shown to converge as[25]

$$\|u^{>\epsilon}-u\|\leqslant O(\epsilon)\|u\|. \tag{18}$$

The dynamic grid adaptation is tightly coupled with the wavelet filter. Due to the one-to-one correspondence between wavelets and grid points, the latter are omitted from the computational mesh if the associated wavelets are omitted from the representation (17). The multilevel structure of this wavelet approximation provides a natural way to obtain the solution on a near optimal numerical grid, which is dynamically adapted to the evolution of the main flow structures, both in location and scale, while higher resolution computations are carried out where (and only where) steep gradients in the resolved flow field occur.

The multi-resolution wavelet decomposition (17) is used for both grid adaptation and interpolation, while a hierarchical finite difference scheme, which takes advantage of the wavelet interpolating properties, is used to differentiate the local function approximations, and to provide the values of derivatives of the function at those particular locations.

III.B. Adaptive-Anisotropic Wavelet Collocation Method

Second-generation wavelet bases described in section III.A rely on topologically rectilinear grids and inherently isotropic mesh elements, which, despite being a highly valuable methodology for the numerical solution of fluid dynamics equations due to mathematical rigor, simplicity and computational efficiency,[26]

puts some limitations on the applicability of the approach. These limitations were recently overcome with the development of the Adaptive-Anisotropic Wavelet Collocation Method (A-AWCM).[24] A-AWCM preserves active error-controlling properties of the original AWCM, but provides additional flexibility to control mesh anisotropy and to solve the problem in complex domains by separating the computational space from the physical one and introducing a mapping between them, thus, allowing the use of anisotropic curvilinear meshes in complex geometries.

The introduction of a function that maps the physical domain, say $\mathbf{x} \in \Omega_p$, to the computational domain, say $\boldsymbol{\xi} \in \Omega_c$, provides the necessary flexibility of the mesh geometry when dealing with wall-bounded flows, such as channel flows and flows around obstacles. In physical space, a more optimal spatial distribution of mesh points can be realized, where mesh element aspect ratios, grid stretching and orientation of the cells can be properly varied. Furthermore, body-fitted meshes can be constructed with the accurate resolution of the boundary layer and wake regions. At the same time, the structured rectilinear assembly of collocation points in the computational space is retained, which allows one to use computationally efficient discrete wavelet transform and derivative approximations.

A-AWCM utilizes a general curvilinear coordinate mapping function $\mathbf{x}(\boldsymbol{\xi})$, which can be either continuous or discrete. The mapping coordinates are viewed as additional variables, which can be adapted on and which can be differentiated in computational space, thus, allowing the construction of the Jacobian matrix

$$\mathcal{J}_{ij} \equiv \frac{\partial x_i}{\partial \xi_j}. \tag{19}$$

Spatial derivatives in physical space are evaluated numerically as

$$\frac{\partial}{\partial x_i} = \frac{\partial \xi_j}{\partial x_i}\frac{\partial}{\partial \xi_j} = \mathcal{J}^{-1}_{ij}\frac{\partial}{\partial \xi_j}, \tag{20}$$

where $\mathcal{J}^{-1}_{ij}$ is the inverse Jacobian matrix. Based on the particular flow structures and flow geometry, mesh anisotropy should be controlled through mapping function or mesh generation, and ideally should take into consideration local flow anisotropy. For instance, more isotropic cells are needed around boundary layer separation points to properly resolve flow physics, while anisotropic meshes should be used in boundary and shear layers. At the same time, additional measures should be taken to avoid the generation of mapping resulting in cells with high skewness, degenerate Jacobian ($\det(\mathcal{J}) \to 0$), or non-smooth mesh lines, since the degradation of the mesh quality can not be fully rectified by the automated mesh refinement. It should be noted that an additional adaptation on physical coordinates can only assure the accuracy of the representation of the physical coordinates and would result in additional mesh refinement in the regions where the mesh is ill-conditioned, but does not guarantee the optimality of the mesh anisotropy, which could be controlled only as a part of mesh generation process.

III.C. A-AWCM with Periodic Boundary Conditions

Special consideration should be given to the case when the physical domain has periodic boundary conditions, since physical coordinates are not periodic. In this case the mesh adaptation can be performed on the coordinate perturbations x_i^{prd} defined by

$$x_i^{\mathrm{prd}} = x_i - \mathcal{J}_{ip}^{\mathrm{prd}}(\xi_p - \min(\xi_p)), \tag{21}$$

where $i = 1, \ldots, n$, repeated index p assumes summation only along periodic directions, and $\mathcal{J}_{ip}^{\mathrm{prd}}$ is the linear (with respect to ξ_p) Jacobian, given by

$$\mathcal{J}_{ip}^{\mathrm{prd}} = (\, x_i|_{\xi_p=\max(\xi_p)} - x_i|_{\xi_p=\min(\xi_p)})/(\max(\xi_p) - \min(\xi_p)). \tag{22}$$

Note that for simply translated periodic boundaries x_i^{prd} is constant. Rewriting Eq. (21) for x_i and substituting into Eq. (19) results in the following Jacobian matrix

$$\mathcal{J}_{ij} = \frac{\partial x_i^{\mathrm{prd}}}{\partial \xi_j} + \mathcal{J}_{ip}^{\mathrm{prd}}\delta_{pj} + \frac{\partial \mathcal{J}_{ip}^{\mathrm{prd}}}{\partial \xi_j}(\xi_p - \min(\xi_p)), \tag{23}$$

where index p assumes summation only in periodic directions. Note that the linear Jacobian (22) is not a function of ξ_p, resulting in $\dfrac{\partial \mathcal{J}^l_{ip}}{\partial \xi_j} = 0$ if $j = p$, while the term $\mathcal{J}_{ij}^{\mathrm{prd}} = 0$ when j is the non-periodic direction.

IV. Variable Thresholds and Novel Adaption Strategy.

The family of DES models, for instance the DDES model, provides a unified model form with hybrid length scales transitioning between the LES and RANS regime. As explained in section I, two distinct levels of thresholds for the Adaptive LES and W-URANS should be used respectively for computations using these two different methods. Using a uniform wavelet threshold ϵ at the value of either the Adaptive LES or W-URANS is inappropriate. The accuracy of the simulation in the RANS regime is lost if an aggressively high level of ϵ of the Adaptive LES is used. In contrast, a small ϵ as low as in W-URANS automatically switches Adaptive LES to the WDNS regime and, thus, is also unacceptable. Therefore, a variable wavelet threshold strategy that blends two distinct regions of DDES model is required and is the subject of this paper. Since the DDES model already makes use of the blending function f_d, which switches between the length scales l_{RANS} and l_{LES} in Eq. (11) and serves as a good indicator between two regimes, it is natural to use the same blending function for interpolation between the high ϵ_{LES} and low ϵ_{RANS} in Adaptive LES and RANS regions, respectively:

$$\epsilon_{\text{hyb}} = (1 - f_d)\epsilon_{RANS} + f_d\epsilon_{LES} \tag{24}$$

The threshold field ϵ_{hyb} is used to perform grid adaptation in the A-AWCM method. In general, the quantities that dominate and drive the physics of the flow must be well resolved, and thus the grid adaptation should be performed based on scales of these quantities using Eq. (17). For instance, for wall-bounded compressible turbulent flows with isothermal wall boundaries, the velocity, total energy and temperature are appropriate quantities to be adapted.

This strategy by itself does not work well. When turbulence contents are developed, for example in a plane channel flow, fluctuations exist in both the RANS and LES regions even though the intensity of fluctuations of the former is lower than the latter. In other words, the flow structures in the RANS region near the wall are not as smooth as those in a W-URANS simulation. Therefore, a relatively low threshold ϵ_{RANS} would cause an unnecessary increase of grid points below the log-layer region and the expected efficiency of a hybrid-model method would be lost. Recall that the reason for the low threshold ϵ_{RANS} is the mean quantities in the RANS equations. In the DDES case, all variables become instantaneous, and dynamically evolved turbulent eddies are intended to be resolved. The low threshold ϵ_{RANS} is no longer a good choice to adapt on the primary unknown variables of the evolution equations. In order to deal with this difficulty, a novel adaptation strategy is proposed and consists of following steps:

1. using ϵ_{hyb} in Eq. (24), adapt on the instantaneous variables during the early transient stage and calculate the statistical mean quantities averaged over the same period,

2. decompose instantaneous quantities into mean and fluctuation components after the LES contents are developed and the accumulated mean quantities become smooth,

3. calculate scales, say the L_2 norm, for both the mean and fluctuation components, and using the original ϵ_{hyb} adapt on both the mean quantities and the fluctuation quantities but with the increased threshold level for the latter.

This new adaptation procedure is very effective in reducing the degrees of freedom. For the time being, the accuracy of the mean quantities preserves particularly in the RANS regions. A supersonic turbulent channel flow case with the wavelet-based adaptive DDES method described above using the new adaptation procedure is tested. The effect of this adaptation procedure is illustrated in Figure 1. Adaptive grid points colored by resolution levels at the solid wall by different adaptation strategies are depicted. Note that adapted quantities are momentum components, total energy and temperature. Since momentum and temperature are constant at the wall, perturbations exist only in the total energy that contains the density. Instantaneous quantities in Figure 1(a) and mean quantities in Figure 1(b) use $\epsilon_{RANS} = 2.5 \times 10^{-3}$ and $\epsilon_{LES} = 5.0 \times 10^{-2}$. For the fluctuation fields in Figure 1(b), increased thresholds $\epsilon_{RANS} = 1.25 \times 10^{-2}$ and $\epsilon_{LES} = 2.5 \times 10^{-1}$ are prescribed for testing purpose.

Figure 1(a) has substantially more grid points retained at the wall than Figure 1(b), while the total number of active grid points for the former is 3.2 million, it is 2.2 million for the latter. Considerable reduction of grid points for the latter case arises from much sparser representation in the near wall RANS region. In the middle part of the channel, adaptive meshes are similar for both cases. Considering the mean and fluctuation components separately using different levels of effective wavelet filter threshold is thereby beneficial to retain the accuracy and gain the efficiency. As the solution becomes statistically converged, the

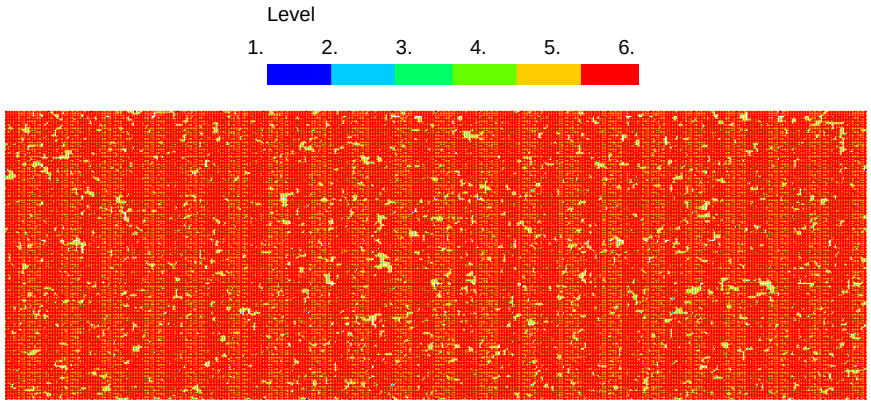

(a) Adaption on the instantaneous quantities.

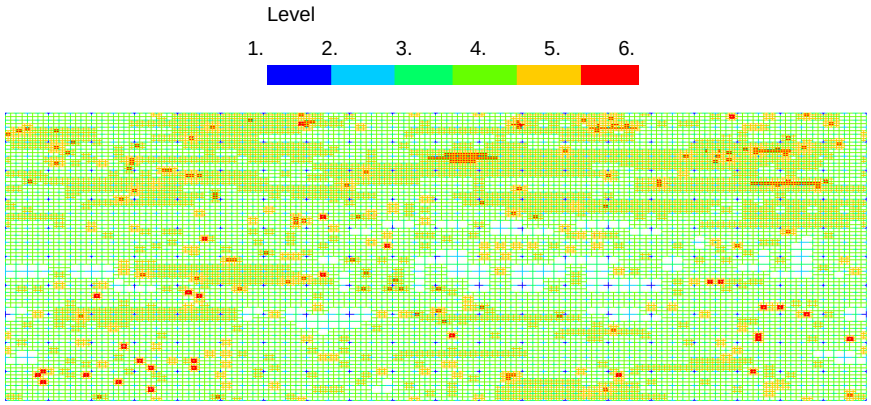

(b) Adaption on the mean and fluctuation quantities.

Figure 1. Adaptive grids points colored by resolution levels at the solid wall. Horizontal direction is the stream-wise direction and the vertical direction is the span-wise direction.

averaged fields are smoother. Accordingly, the thresholds for mean quantities can be smaller and the ones for fluctuations can be larger without loss of accuracy for the mean value. Overall, the degrees of freedom can potentially be reduced further since the grid points retained to resolve the turbulent fulctuations are dominant.

Details of the simulation setup and results are presented below in section V. One may argue here that DDES is known to be inappropriate for plane channel flow cases due to the log-layer mismatch (LLM)[20,27] for attached flows. However, as stated above, the task of the current work is to investigate the coexistence of W-URANS and adaptive LES. If the wavelet-based adaptive DDES method works effectively and efficiently and produces similar or even better results with non-adaptive DDES, this approach could be easily applied to separated flow, which is the ongoing work.

V. Simulations and Results

V.A. Supersonic channel flows

In this subsection, a simulation of a supersonic channel flow is presented for testing of the wavelet-based DDES turbulence modeling approach and the novel grid adaptation strategy described in section IV. Fourth

order wavelets and finite difference scheme are used for the discrete wavelet transform and interpolation, and derivative approximations. For the time integration, the explicit standard four-stage Runge-Kutta scheme is applied with the CFL= 0.5. The grid adaptation is performed on mean (Reynolds-averaged) and fluctuation components of momentum, total energy and temperature scaled by L_2 norm. Specifically, the three components of momentum share a single scale that is calculated by the corresponding mean and fluctuation momentum magnitudes rather than using the scale of each individual component in the x, y and z directions, respectively. The fluctuations of the total energy and temperature are evaluated by the Reynolds fluctuation root mean square. The wavelet filter thresholds for the mean quantities are $\epsilon_{RANS} = 2.5 \times 10^{-3}$ and $\epsilon_{LES} = 5.0 \times 10^{-2}$, while increased thresholds $\epsilon_{RANS} = 1.25 \times 10^{-2}$ and $\epsilon_{LES} = 2.5 \times 10^{-1}$ are prescribed for all fluctuation quantities.

It is worth noting that since the Reynolds average fields start to be computed from the early transient stage, an exponentially weighted time average method is employed instead of the simple ensemble average. Given an instantaneous quantity ϕ, the corresponding Reynolds average quantity is denoted as $\langle\phi\rangle$, which reads

$$\langle\phi\rangle(t) \equiv \int_{-\infty}^{t} \phi(t') \frac{1}{t_s} e^{-(t-t')/t_s} dt'. \tag{25}$$

Differentiating Eq. (25) gives

$$\frac{d\langle\phi\rangle}{dt} = \frac{1}{t_s}(\phi - \langle\phi\rangle). \tag{26}$$

Using first order approximation, Eq. (26) can be numerically evaluated as

$$\langle\phi\rangle^n = \alpha\phi^n + (1-\alpha)\langle\phi\rangle^{n-1}, \tag{27}$$

$$\alpha = \frac{\Delta t}{\Delta t + t_s}. \tag{28}$$

where Δt is the time integration interval and t_s is the time scale for the averaging. For the present channel flow case one flow through time (FTT), t_{FTT}, is used for t_s. A certain Reynolds fluctuation quantity is referred to as $\phi' = \phi - \langle\phi\rangle$. A Favre average quantity is signified as $\{\phi\} = \langle\rho\phi\rangle/\langle\rho\rangle$ while the corresponding Favre fluctuation variable is denoted as $\phi'' = \phi - \{\phi\}$.

The computational domain size is $4\pi H \times 2H \times 4\pi H/3$ in steam-wise(x), wall-normal(y) and span-wise(z) directions, respectively, where H is the half height of the channel. The bulk Reynolds number is $Re = \rho_b u_b H/\mu_w$, and the Mach number is $Ma = u_b/c_w$, where $(\cdot)_b$ and $(\cdot)_w$, respectively, denote bulk mean quantities and quantities averaged at the walls, while c is the speed of sound. The friction Reynolds number is $Re_\tau = \rho_w u_\tau H/\mu_w$, where $u_\tau = \sqrt{\tau_w/\rho_w}$. Here, τ_w indicates the wall shear stress. Two different flow configurations are considered, *i.e.* $Re = 3000$ with $Ma = 1.5$ (CH1) and $Re = 6000$ with $Ma = 3.0$ (CH2). A feedback control of the body force in the stream-wise direction based on the bulk mass flow rate is employed to maintain the desired flow rate. Once the statistically steady state regime is achieved, the feedback is turned off and the statistics start to be recalculated. The initial conditions are: the laminar parabolic velocity profile for plane channel flows, uniform density and total energy. Initial condition for $\tilde{\nu}$ has a prescribed value at the wall and exponentially approaches to a uniform value in the free stream. In order to accelerate the transition to fully developed turbulence, the least stable modes of the two-dimensional Orr-Sommerfield solution are superimposed as velocity perturbations in the x and y directions along with smooth random noises in the y and z directions.

The discretization of the computational domain is done by using dyadic nested wavelet collocation grids for the wavelet decomposition (17). The computational mesh has $J = 6$ and an effective (finest level) resolution of $640 \times 244 \times 320$ with base (coarsest level) grids with resolution of $20 \times 7 \times 10$. Using A-AWCM, the mesh is stretched in the wall normal direction following a hyperbolic tangent distribution. For the finest level of resolution, the first wall normal grid spacing is $\Delta y(1)^+ = 0.29$ with a corresponding stretching ratio equal to 1.04. The x and z directions have the periodic boundary condition with grid points evenly distributed. A feedback control of the body force in the stream-wise direction based on the bulk mass flow rate is employed to maintain the desired flow rate. The grid aspect ratios in the immediate vicinity of the wall are $\Delta x^+/\Delta y^+ = 15$ and $\Delta z^+/\Delta y^+ = 10$. The grid compression ratio, defined as the percentage of collocation points discarded in the adaptive grid (2.5 million) compared to the number of non-adaptive grid points, is to 95.0%. An Adaptive LES study[28] for the same channel flow case has active grid points of 3.5 million with an aggressive uniform threshold $\epsilon = 0.1$ adapting on instantaneous momentum, total energy

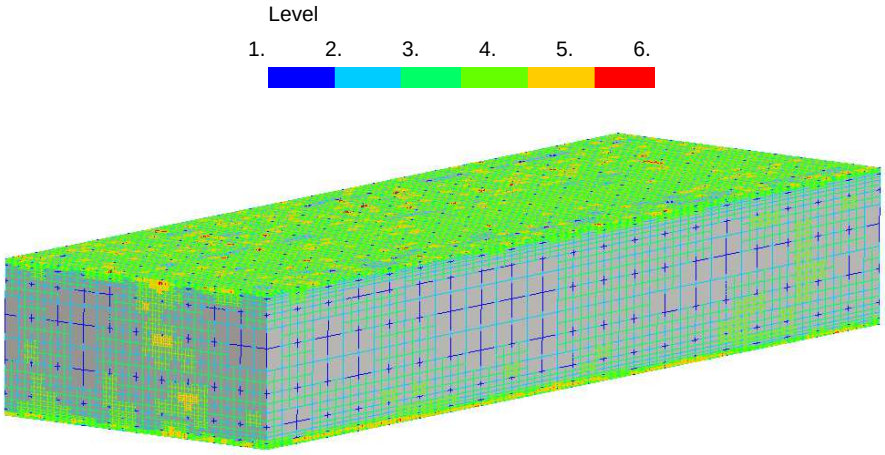

Figure 2. The adaptive grids on the surfaces of the physical domain.

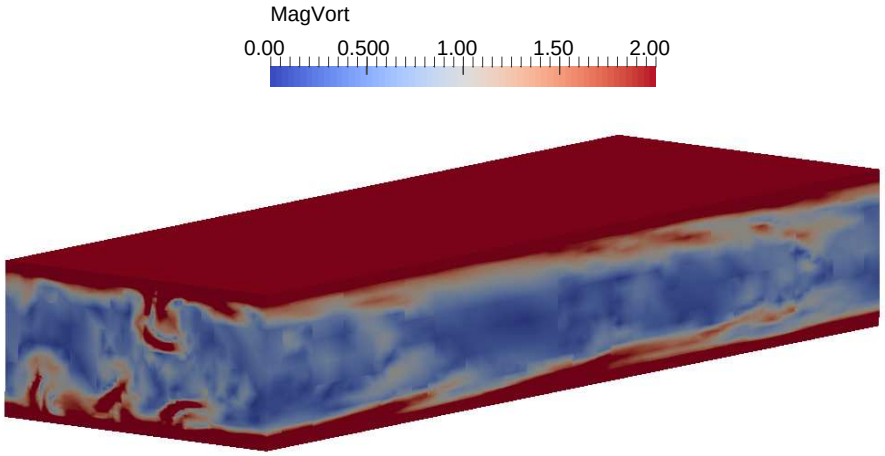

Figure 3. The vorticity magnitude contours on the surfaces of the physical domain.

and temperature. Both the accuracy indicated by the threshold and efficiency in terms of degrees of freedom for the novel adaptation strategy are successfully gained.

The adaptive grid for the developed turbulent flow field is illustrated in Figure 2, demonstrating refinement around localized structures visualized by the vorticity magnitude contours in Figure 3. The mean and turbulence statistics profiles are plotted in Figure 4–6. Statistics are computed by interpolating the continuous wavelet basis onto 2D, nonadaptive sampling grids, and averaging along the stream-wise direction in each 2D slide and then across multiple slides over a long time period with exponentially decaying weights. Therefore all curves plotted below show the stream-wise, span-wise and time averaged quantities of the W-DDES solution. Due to the high Mach number and iso-thermal boundary condition, temperature within the channel increases because of the viscous dissipation heating. It appears that the thermodynamic related quantities, namely the density and total energy, converge more slowly than the momentum.

The friction Reynolds number Re_τ predicted by the W-DDES is 212, 4.0% underestimated compared with the benchmark DNS results,[29–31] $Re_\tau = 221$. Two sources exist for this error. The first is the ϵ_{hyb} for the mean quantities. The second is the LLM issue of DDES, where the interception of the log-law velocity profiles predicted in the LES regime of the DDES model is higher than that in the RANS regime, though both regimes share the same log-law slope. This issue may introduce an underestimation of the friction up to 15%.[20] However, our predicted Re_τ is obviously much better than a typical LLM result by the conventional

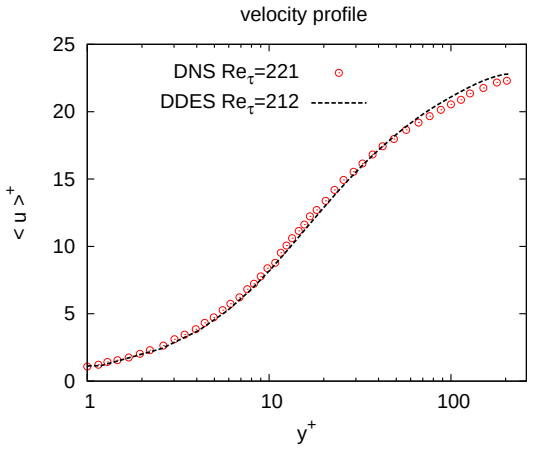

(a) Velocity profiles. DNS data from Ref. 29.

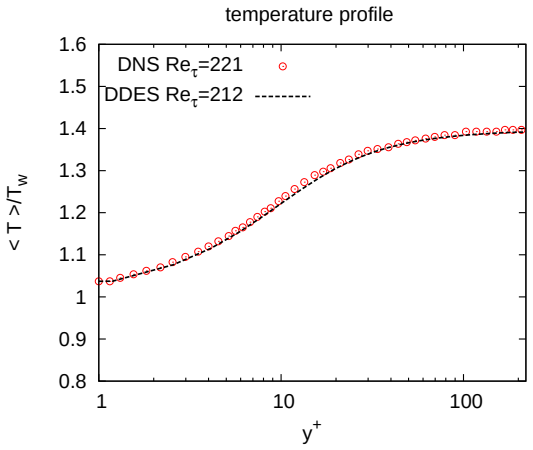

(b) Temperature profiles. DNS data from Ref. 30.

Figure 4. Mean profiles comparison between W-DDES and DNS results.

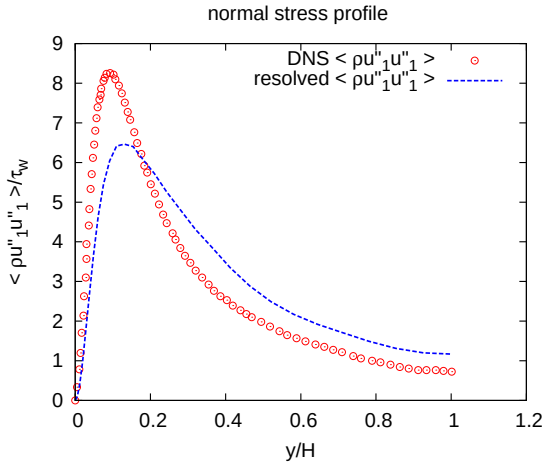

(a) Resolved turbulent normal stress profiles by DDES and comparison with the DNS data from Ref. 31.

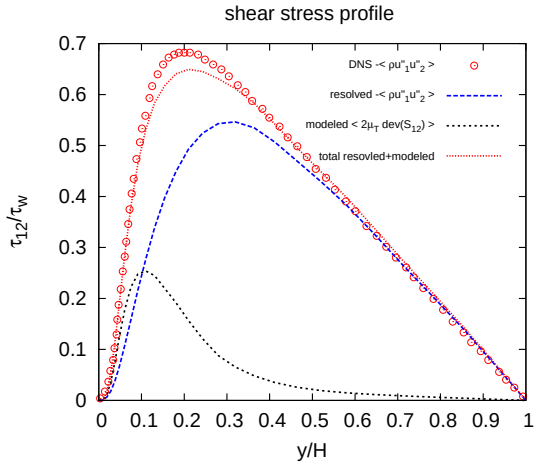

(b) Resolved, modeled and total turbulent shear stress profiles by DDES and comparison with the DNS data from Ref. 31.

Figure 5. Turbulent stresses profiles comparison between W-DDES and DNS results.

DDES. In fact, it is even better than the result of the wavelet-based adaptive wall resolved LES, $Re_\tau = 205$ as reported in Ref. 28. Moreover, the Reynolds mean velocity and temperature profile shown in Figure 4 agree quite well with the DNS data. The LLM happens to be eliminated by a significant overestimation of the resolved part of the turbulent normal stress $\langle \rho u_1'' u_1'' \rangle$ as plotted in Figure 5(a). This can be explained by the benefit of the wavelet-based adaptive method where the local mesh refinement in the LES region results in high levels of resolved turbulent stresses, and hence more momentum can be transported into the lower portion of the boundary layer. On the contrary, the conventional non-adaptive DDES predicts relatively low levels of resolved turbulent stresses, while it excessively damps out turbulence at the RANS-LES interface, located at the log-law region.

As argued in section IV, the current work aims to show the capability for the coexistence of the W-RANS and adaptive LES regimes within the A-AWCM framework. Our results successfully demonstrate the feasibility of the novel W-DDES modeling approach proposed in this work.

Figure 5(b) depicts the resolved, modeled and total turbulent shear stress $-\langle \rho u_1'' u_2'' \rangle$ compared with the DNS data. Note that modeled normal stress is negligible in Figure 5(a) because of the small mean velocity gradient $\partial_x \langle u_1 \rangle$. Similar to the turbulent normal stress, the predicted shear stress is slightly underestimated around the RANS-LES interface layer where $y^+ \approx 20$ to 50. In addition, the predicted peak of the maximum

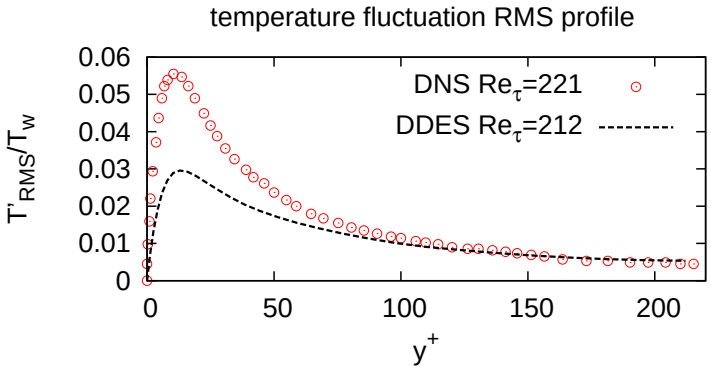

Figure 6. Reynolds fluctuation root mean square of the temperature field and comparison with the DNS data.[30]

value of the turbulent normal stress component shown in Figure 5(a) is slightly closer to the middle of the channel than the DNS data. From these observations, the issue of damping of turbulence at the RANS-LES interface for conventional low resolution non-adaptive DDES[27] still exists. The Reynolds fluctuation root mean square temperature profiles plotted in Figure 6 illustrate an underestimation of temperature fluctuation compared with the DNS data. Note that the turbulent heat flux is modeled through a Reynolds analogy as in Eq. 6 with a constant turbulent Prandtl number, $Pr_T = 0.9$, the temperature fluctuations are not well modeled, as opposed to the eddy viscosity and the Reynolds stresses. So the result in Figure 6 is not unaccepted. The fact that we partially resolve the temperature fluctuations, makes the approach closer to LES than RANS where the flucation should be zero.

It is worth emphasizing the importance of using the absolute wavelet thresholding scale $\|u\|$ smoothly varying in time. Turbulent fluctuations are highly intermittent in nature. As a result, the instantaneous scales of the fluctuating components also vary in time. A rapid increase of the absolute thresholding scale could result in excessive filtering of turbulent fluctuations in the LES region and the expansion of RANS region, which, in turn, could manifest itself in the log-layer mismatch. In the simulations discussed above, the time averaged scales given by discrete version Eq. 26 of Eq. 25 are used, with $t_s \approx 0.1 t_{\mathrm{FTT}}$.

A possible appearance of the LLM solution when the instantaneous absolute thresholding scales are used is demonstrated in Figure 7. The discrepancy of the mean stream-wise velocity profiles is significant as shown in Figure 7(a). The excessive filtering of fluctuating components in LES region results in the under-resolution of turbulent shear stress as shown in Figure 7(b), which causes an excessive underestimation of the total shear stresses. It should be noted that when the instantaneous absolute thresholding scales are used, the solution switches between two branches: one with the LLM issue and the other without. Figure 8 shows the mechanism of the two-branch solutions when the instantaneous absolute thresholding scales are used. A typical LLM solution produces relatively higher values of eddy viscosity and lower values of resolved Reynolds stresses or fluctuations. Therefore the adaptive criterion of the wavelet coefficient based on the instantaneous fluctuation quantities is loosen and more grid points are retained. Meanwhile, more grid points, in turn, suppress the eddy viscosity and hence enhance the resolved Reynolds stresses, which finally leads to a more accurate solution without LLM. However, when the fluctuation components are increased, more grid points are discarded, resulting in coarsening of the adaptive grid and the solution driven back to typical LLM branch. When using time averaged absolute thresholding scales, no LLM is observed and solutions for LES and RANS branches match and converge to the statistically steady solution presented in Figure 4, 5 and 6.

VI. Conclusions

A novel Wavelet-based adaptive Delayed Detached Eddy Simulation (W-DDES) approach for simulations of wall-bounded compressible turbulent flows is proposed. Its effectiveness is demonstrated for flow simula-

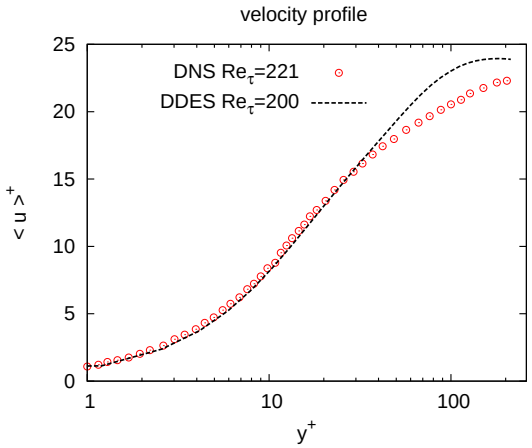

(a) Velocity profiles. DNS data from Ref. 29.

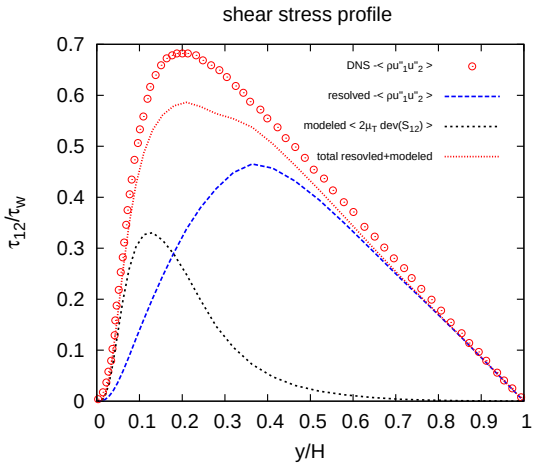

(b) Resolved, modeled and total turbulent shear stress profiles by DDES and comparison with the DNS data from Ref. 31.

Figure 7. Turbulent stresses profiles comparison between W-DDES with log-layer mismatch and DNS results.

Case	Without LLM	With LLM	Adaptive LES
Total grid points	2.8M	2.0M	3.5M
Eddy viscosity μ_T			
Scales of fluctuation/ Reynolds stresses			
Re_τ (=221 DNS)	214	200	205

Figure 8. Schematic of the mechanism of the two-branch solutions when instantaneous quantity scales are used for wavelet filter thresholding. A typical LLM solution produces relatively higher values of eddy viscosity and lower values of resolved Reynolds stresses or fluctuations. Therefore the adaptive criterion of the wavelet coefficient based on the instantaneous fluctuation quantities is loosen and more grid points are retained. Meanwhile, more grid points, in turn, suppress the eddy viscosity and hence enhance the resolved Reynolds stresses, which finally leads to a more accurate solution without significant LLM. However, when the fluctuation components have increased, more grid points are discarded. This way the adaptive grid will be locally coarsened, and drive the solution back to typical LLM branch. Adaptive LES data from Ref. 28 as reference.

tions using the Spalart-Allmaras DDES model. A variable wavelet thresholding strategy blending two distinct thresholds for the Reynolds-averaged Navier-Stokes (RANS) and Large-Eddy Simulation (LES) regimes is used. A novel mesh adaptation on mean and fluctuation quantities with different wavelet thresholds levels is proposed. Both the accuracy indicated by the threshold and efficiency in terms of degrees of freedom for the novel adaptation strategy are successfully achieved compared with the wavelet-based adaptive LES method, in which the adaptation is performed on instantaneous quantities using *a priori* defined uniform thresholds. Moreover, the newly proposed W-DDES resolves the typical log-layer match issue encountered in the conventional non-adaptive DDES method thanks to the benefit of the local mesh refinement of this adaptive wavelet-based method. To avoid a two-branch-solution with switching between branches with and without the log-layer mismatch, the time averaged absolute thresholding scales should be used. Simulations of separated flows using the W-DDES method are currently underway and will be reported in the future. The current study serves as a crucial step towards construction of a unified wavelet-based adaptive hierarchical RANS/LES modeling framework, capable of performing simulations of varying fidelities from no-modeling direct numerical simulations to full-modeling RANS simulations.

Acknowledgments

This work is supported by NASA's Revolutionary Computational Aerosciences (RCA) discipline under the Transformational Tools and Technologies (TTT) Project Grant No NNX15AU24A. OVV was supported by Russian Science Foundation (Project 16-11-10350). Authors are also thankful for the computing time on NSF XSEDE Stempede and Comet systems and RCC HPC system at Florida State University.

References

[1]Vasilyev, O. V. and Bowman, C., "Second-generation wavelet collocation method for the solution of partial differential equations," *Journal of Computational Physics*, Vol. 165, No. 2, 2000, pp. 660–693.

[2]Vasilyev, O. V., "Solving multi-dimensional evolution problems with localized structures using second generation wavelets," *International Journal of Computational Fluid Dynamics*, Vol. 17, No. 2, 2003, pp. 151–168.

[3]Vasilyev, O. V. and Kevlahan, N. K.-R., "An adaptive multilevel wavelet collocation method for elliptic problems," *Journal of Computational Physics*, Vol. 206, No. 2, 2005, pp. 412–431.

[4]Souopgui, I., Wieland, S. A., Hussaini, M. Y., and Vasilyev, O. V., "Space–time adaptive approach to variational data assimilation using wavelets," *Journal of Computational Physics*, Vol. 306, 2016, pp. 253–268.

[5]Nejadmalayeri, A., Vezolainen, A., Brown-Dymkoski, E., and Vasilyev, O. V., "Parallel adaptive wavelet collocation method for PDEs," *Journal of Computational Physics*, Vol. 298, 2015, pp. 237–253.

[6]Farge, M., Schneider, K., Pellegrino, G., Wray, A. A., and Rogallo, R. S., "Coherent vortex extraction in three-dimensional homogeneous turbulence: Comparison between CVS-wavelet and POD-Fourier decompositions," *Physics of Fluids (1994-present)*, Vol. 15, No. 10, 2003, pp. 2886–2896.

[7]Goldstein, D. E. and Vasilyev, O. V., "Stochastic coherent adaptive large eddy simulation method," *Physics of Fluids*, Vol. 16, No. 7, 2004, pp. 2497–2513.

[8]Goldstein, D. E., Vasilyev, O. V., and Kevlahan, N., "Feasibility Study of an Adaptive Large Eddy Simulation Method," *AIAA Paper*, 2003, pp. 2003–3551.

[9]Goldstein, D. E., Vasilyev, O. V., and Kevlahan, N. K.-R., "CVS and SCALES simulation of 3-D isotropic turbulence," *Journal of Turbulence*, , No. 6, 2005, pp. N37.

[10]Kevlahan, N. K. and Vasilyev, O. V., "An adaptive wavelet collocation method for fluid-structure interaction at high Reynolds numbers," *SIAM Journal on Scientific Computing*, Vol. 26, No. 6, 2005, pp. 1894–1915.

[11]Kevlahan, N.-R., Vasilyev, O., Goldstein, D., and Jay, A., "A three-dimensional adaptive wavelet method for fluid-structure interaction," *Direct and Large-Eddy Simulation V*, Springer, 2004, pp. 147–154.

[12]Vasilyev, O. V. and Kevlahan, N.-R., "Hybrid wavelet collocation–Brinkman penalization method for complex geometry flows," *International journal for numerical methods in fluids*, Vol. 40, No. 3-4, 2002, pp. 531–538.

[13]De Stefano, G. and Vasilyev, O. V., "A fully adaptive wavelet-based approach to homogeneous turbulence simulation," *Journal of Fluid Mechanics*, Vol. 695, 2012, pp. 149–172.

[14]Nejadmalayeri, A., Vezolainen, A., De Stefano, G., and Vasilyev, O. V., "Fully adaptive turbulence simulations based on Lagrangian spatio-temporally varying wavelet thresholding," *Journal of Fluid Mechanics*, Vol. 749, 2014, pp. 794–817.

[15]De Stefano, G., Nejadmalayeri, A., and Vasilyev, O. V., "Wall-resolved wavelet-based adaptive large-eddy simulation of bluff-body flows with variable thresholding," *Journal of Fluid Mechanics*, Vol. 788, 2016, pp. 303–336.

[16]De Stefano, G., Brown-Dymkoski, E., and Vasilyev, O. V., "Wavelet-based adaptive unsteady Reynolds-averaged turbulence modeling of external flows," To appear in *Journal of Fluid Mechanics*, 2018.

[17]Liu, Q. and Vasilyev, O. V., "A Brinkman penalization method for compressible flows in complex geometries," *Journal of Computational Physics*, Vol. 227, No. 2, 2007, pp. 946–966.

[18]De Stefano, G. and Vasilyev, O. V., "Wavelet-based adaptive simulations of three-dimensional flow past a square cylinder," *Journal of Fluid Mechanics*, Vol. 748, 2014, pp. 433–456.

[19]De Stefano, G., Goldstein, D. E., and Vasilyev, O. V., "On the role of subgrid-scale coherent modes in large-eddy simulation," *Journal of Fluid Mechanics*, Vol. 525, 2005, pp. 263–274.

[20]Spalart, P. R., Deck, S., Shur, M., Squires, K., Strelets, M. K., and Travin, A., "A new version of detached-eddy simulation, resistant to ambiguous grid densities," *Theoretical and computational fluid dynamics*, Vol. 20, No. 3, 2006, pp. 181–195.

[21]Spalart, P., Jou, W., Strelets, M., Allmaras, S., et al., "Comments on the feasibility of LES for wings, and on a hybrid RANS/LES approach," *First AFOSR international conference on DNS/LES, Ruston, Louisiana*, Vol. 1, Greyden Press, Columbus, OH, 1997, pp. 4–8.

[22]Shur, M., Spalart, P., Strelets, M., and Travin, A., "Detached-eddy simulation of an airfoil at high angle of attack," *Engineering turbulence modelling and experiments*, Vol. 4, 1999, pp. 669–678.

[23]Spalart, P. and Allmaras, S., "A one-equation turbulence model for aerodynamic flows," *30th aerospace sciences meeting and exhibit*, 1992, p. 439.

[24]Brown-Dymkoski, E. and Vasilyev, O. V., "Adaptive-Anisotropic Wavelet Collocation Method on general curvilinear coordinate systems," *Journal of Computational Physics*, 2017.

[25]Donoho, D. L., "Interpolating Wavelet Transforms," Tech. Rep. 408, Department of Statistics, Stanford University, 1992.

[26]Schneider, K. and Vasilyev, O. V., "Wavelet methods in computational fluid dynamics," *Annual Review of Fluid Mechanics*, Vol. 42, 2010, pp. 473–503.

[27]Shur, M. L., Spalart, P. R., Strelets, M. K., and Travin, A. K., "A hybrid RANS-LES approach with delayed-DES and wall-modelled LES capabilities," *International Journal of Heat and Fluid Flow*, Vol. 29, No. 6, 2008, pp. 1638–1649.

[28]Brown-Dymkoski, E., *Adaptive Wavelet-Based Turbulence Modeling for Compressible Flows in Complex Geometry*, Ph.D. thesis, Department of Mechanical Engineering, University of Colorado at Boulder, 2016.

[29]Coleman, G. N., Kim, J., and Moser, R., "A numerical study of turbulent supersonic isothermal-wall channel flow," *Journal of Fluid Mechanics*, Vol. 305, 1995, pp. 159–183.

[30]Morinishi, Y., Tamano, S., and Nakabayashi, K., "Direct numerical simulation of compressible turbulent channel flow between adiabatic and isothermal walls," *Journal of Fluid Mechanics*, Vol. 502, 2004, pp. 273–308.

[31]Foysi, H., Sarkar, S., and Friedrich, R., "Compressibility effects and turbulence scalings in supersonic channel flow," *Journal of Fluid Mechanics*, Vol. 509, 2004, pp. 207–216.